Available online at www.sciencedirect.com
ScienceDirect
Journal of Nuclear Materials 367–370 (2007) 1458–1462
journal of nuclear materials
www.elsevier.com/locate/jnucmat

Thermal stability and nano-structure of metal-doped carbon layers

M. Balden [a,*], C. Adelhelm [a], M. Sikora [b,c]

[a] Max-Planck-Institut für Plasmaphysik, EURATOM Association, D-85748 Garching, Germany
[b] AGH University of Science and Technology, Al. Mickiewicza 30, 30-059 Krakow, Poland
[c] European Synchrotron Radiation Facility, 6 rue Jules Horowitz, 38043 Grenoble, France

Abstract

Carbon layers doped with Ti, V, W, and Zr to about 15 at.% were produced by means of magnetron sputter deposition, which distributes metal atoms homogeneously in the amorphous carbon matrix. The effects of thermal annealing to temperatures of 500–1300 K on the phase, crystallinity and distribution of the dopant were determined. X-ray diffraction (XRD), MeV ion beam analysis (IBA), and extended X-ray absorption fine-structure spectroscopy (EXAFS) were used for characterization. The three techniques deliver complementary information on different length scales of the diffusion and crystallization. All four metal dopants are in carbidic state with crystallites on the nanometer scale after annealing to 1100 K. Dopant diffusion of no more than 20 nm, even after heating at 1300 K for 2 h, was observed.

1. Introduction

The plasma-facing walls of thermonuclear fusion devices are subjected to erosion, implantation of hydrogen isotopes, and re-deposition of eroded material. The major disadvantage of carbon as plasma-facing material is its intense chemical reactivity with hydrogen (and oxygen), resulting in high erosion yield due to chemical erosion and the ability to trap large amounts of hydrogen in re-deposited layers. Nevertheless, carbon is still the material chosen for the strike point position in the present ITER design [1,2] because of its superior thermomechanical properties, especially its high thermal shock resistance when fibre reinforced [3].

Several studies are addressed to the potential of reducing the chemical erosion yield by doping of carbon-based materials [4–10]. One strategy to relax the constraints for using carbon is to reduce erosion, the source term for the re-deposited carbon layers with their high hydrogen isotope content (tritium in-vessel inventory) [11]. Other strategies are the removal of the tritium containing layers and the creation of carbon layers in desired regions [12,13]. If the reported reductions of the erosion yield by one order of magnitude [14,15] converts directly to a ten times slower accumulation of tritium in the re-deposited layers, constraints for cleaning procedures are strongly relaxed [11].

Re-deposited layers in fusion plasma devices will contain all elements which are accessible by the

* Corresponding author. Tel.: +49 89 3299 1688; fax: +49 89 3299 1212.
E-mail address: Martin.Balden@ipp.mpg.de (M. Balden).

0022-3115/$ - see front matter © 2007 Elsevier B.V. All rights reserved.
doi:10.1016/j.jnucmat.2007.04.019

plasma, including the dopant. The composition of these mixed layers will be dependent on the source terms, which depend on particle and energy impact on each wall section, and the transport of the elements by the plasma. The properties of the mixed layers could dramatically vary from those of 'pure' carbon layers, e.g., their erosion by hydrogen impact, their trapping of hydrogen, or their removal behaviour [15,16].

Investigations of the properties of mixed layers under controlled conditions are of great interest. Therefore, the layer must be well characterized with the starting point being the production of mixed layers and changes by thermal annealing as well as their chemical erosion by hydrogen impact. Magnetron sputter deposition of metal-doped carbon layers simulates the deposition process that takes place in a fusion plasma environment. In both cases, material arrives at the substrate (wall) mainly as single atoms.

In this study, the preparation and characterization of nano-dispersed metal-doped carbon layers are presented with special emphasis on the thermal stability of the dopant phase and its crystallinity and distribution. The chemical erosion of these layers is reported elsewhere [15,17]. The thermal behaviour may be of interest for investigation of the catalytic effect of metal on the graphitization of carbon [18,19].

2. Experimental

Pure carbon layers and layers doped with Ti, V, W, and Zr were prepared by dual-source magnetron sputter deposition. The layers were deposited on silicon and graphite substrates. More details about deposition parameters can be found elsewhere [20].

All data on doped layers were obtained from sandwiched doped layers with around 15 at.% metal concentration between two pure carbon layers. These *triple layers* consisted of ~300 nm pure carbon on the substrate, followed by a ~300 nm thick doped layer, and a ~200 nm sealing of pure carbon. The doped layer was produced by switching on and off the metal sputter source, while carbon was continuously deposited. Prior to the deposition, cleaning with argon plasma etching was performed. Additionally, *quintuple layers* of alternating pure carbon (three) and pure metal (two) layers were produced.

On the triple layers, two equivalent interfaces between doped and pure carbon existed, the carbon was in a comparable state on both sides of the interface (no substrate effect), and possible surface segregation and oxidation effects during the annealing were avoided. The triple layers were annealed to temperatures between 500 and 1300 K in vacuum. The dwell time at the desired temperature was 0.25 or 2 h. The quintuple layers were heated higher, to 1770 K for 0.5 h in helium atmosphere.

Composition, thickness, and homogeneity in depth of the layers were determined by ion backscattering of 0.8–4.0 MeV ^{4}He at a scattering angle of 165° (IBA) [21]. The comparison of 'as-deposited' and annealed layers yielded information on the diffusion of the dopant into the pure carbon layers. This experimental condition resulted in a depth resolution for diffusion of ~20 nm for both interfaces between doped and pure carbon layers.

The crystallographic phase and the crystallite size were investigated with X-ray diffraction (XRD). The phase was evaluated by comparing with the JCPDS ICDD database [22]. The crystallite size was determined by using Scherrer's formula [23] under the assumption that the width of the XRD peak is exclusively determined by the crystallite size.

Information on the local bonding and order around metal atoms were obtained from extended X-ray absorption fine-structure spectroscopy (EXAFS) using synchrotron radiation (beamline A1 and E4, HASYLAB, DESY, Hamburg, Germany). The modulation in the X-ray absorption of the metal atoms is explained by interference of the emitted photo electrons, which were scattered on the surrounding atoms, i.e., the atomic order around the metal atom was sampled [24].

3. Results

3.1. Diffusion of dopant into carbon layer

Fig. 1 shows IBA spectra for a 14 at.% Zr-doped carbon layer 'as-deposited' and after annealing to 1300 K for 0.25 h. The depth distribution of Zr and C and impurities (<2 at.% for O, Ar and <0.05 at.% for Cu, Mo) are observed. No changes due to the annealing are visible, except the release of the argon which was introduced during the deposition. The zirconium diffuses less than ~20 nm into the pure carbon layers, which is the detection limit. Metal diffusion above the detection limit out of the doped layer is not observed for any of the dopants even after annealing up to 1300 K for 2 h. The diffusion for the pure metal layers in the quintuple layers was stronger and easily observable by IBA for

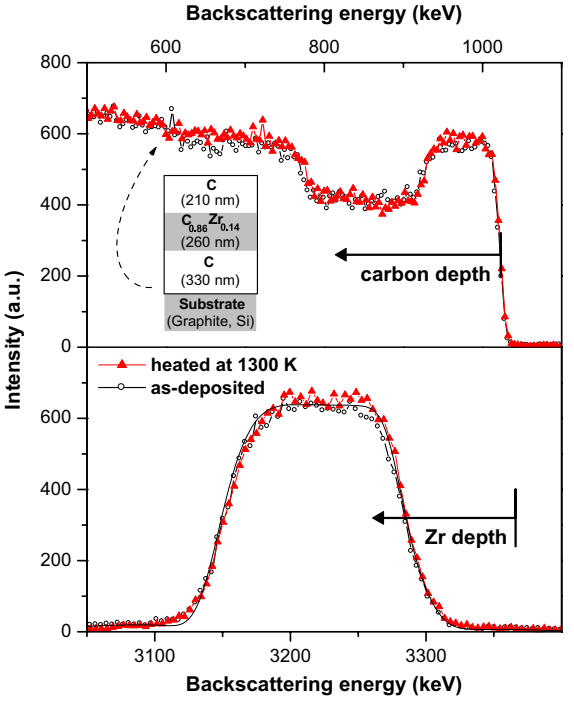

Fig. 1. IBA spectra of 4 MeV ^{4}He from a 14 at.% Zr-doped triple layer 'as-deposited' (open symbols) and after heating at 1300 K for 0.25 h (filled symbols). The energy range containing the information about the carbon (upper level) and zirconium (lower level) are shown. The maximum backscattering energy for each element is marked, for which its depth scale starts (starting point of the solid arrows). The inset sketches the layer structure of the specimen. A simulated spectrum for that sketched specimen is given (line).

all four dopants due to the higher heating temperature (1770 K). The quintuple structure is partly blurred.

3.2. Crystallographic phase and crystallite size

XRD spectra of a 13 at.% V-doped triple layer before and after annealing are given in Fig. 2. In the presented scattering angle range, nearly stoichiometric VC has two strong diffraction peaks. These two peaks grew with annealing temperature and dwell time. The 'as-deposited' specimen does not show any sign of peaks. For phase identification and comparison, a quintuple layer of pure V and C after heating at 1770 K for 0.5 h was investigated, too. The carbon-poor V_8C_7 is the most dominant phase, especially at larger scattering angles. The width of the (222) peak of that quintuple layer gives a crystallite size above 20 nm, the maximal detectable size for the scattering set-up. The deduced crystallite sizes for all annealed V-doped triple layers are given in Fig. 2. The size increases with temperature and dwell time.

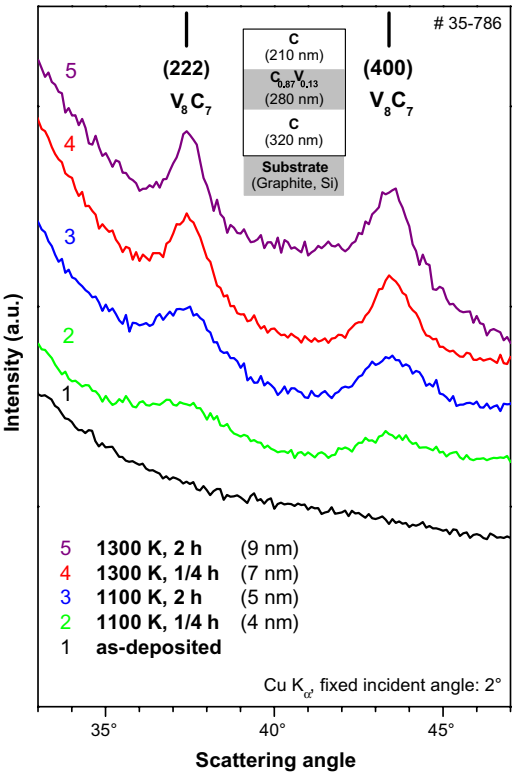

Fig. 2. XRD spectra of 13 at.% V-doped triple layer specimens before and after annealing to 1100 and 1300 K for 0.25 and 2 h. The spectra are shifted vertically for better visibility. The JCPDS ICDD database [22] is used for phase identification, indexing and marking the XRD peaks (#35-786). The crystallite size is obtained from the (222) peak of V_8C_7 by using Scherrer's formula [23] under the assumption that the width of the XRD peak is exclusively determined by the crystallite size. The crystallite sizes are shown. The inset sketches the layer structure of the specimen.

Similar results for Ti and Zr were revealed by XRD investigations. Nearly stoichiometric TiC and ZrC are clearly formed and the crystallite size increases with temperature and dwell time, but the increase is less pronounced for Ti and Zr than for V. The scattering angles of the peaks for the doped layers are the same as for the heated quintuple layers and for TiC and ZrC in the database (#35-784, #32-1383 [22]). The observed phases for these three dopants are in agreement with the published phase diagrams [25].

Tungsten doping leads to different behaviour; e.g., for an 'as-deposited' and 1100 K heated 15 at.% W-doped layer, only one broad peak at ~38° is observed between 30° and 47° scattering

angle, while both, WC and W_2C, should have two and three peaks, respectively, in this range. The width of that peak corresponds to a crystallite size of 2 nm, and does not increase with annealing temperature and dwell time. The scattering angle of this broad peak and two further broad peaks around 61° and 75° fit better to W_2C than to nearly stoichiometric WC. In the heated quintuple specimen with pure tungsten layers, WC is clearly formed in perfect agreement with its reported XRD spectrum (#25-1047 [22]) and in accordance with the phase diagram [25]. The W_2C phase with its reported XRD spectrum (#35-776 [22]) is observed in W-doped fine-grain graphite together with WC. This sample is used as reference for EXAFS.

3.3. Surrounding of metal atoms on atomic scale

In Fig. 3, EXAFS spectra of an annealing series of a 14 at.% Zr-doped triple layer are presented. The spectra are normalized by a standard algorithm (analysis software ATHENA [26]). The EXAFS modulations above the absorption K-edge of zirconium (17995 eV) are clearly getting more pronounced with annealing temperature. They are already looking similar to those of ZrC after heating at 1100 K and are totally different than those of metallic zirconium. By simply noting the pre-edge structure and the exact edge position (inset in Fig. 3), the metal atoms in the 'as-deposited' layer are already in bonding configuration like that of ZrC. The faint modulations in the 'as-deposited' layer suggest an amorphous, disordered region surrounding the metal atoms.

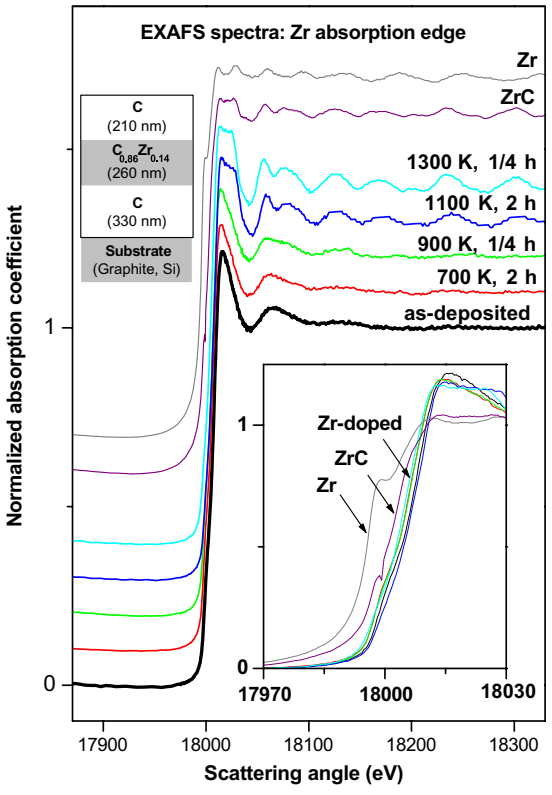

Fig. 3. Normalized EXAFS spectra of 14 at.% Zr-doped triple layers annealed at four temperatures. For comparison, spectra of Zr and ZrC are also shown. The spectra are vertically shifted for better visibility. One inset magnifies the edge position. The other inset sketches the layer structure of the specimen.

The results for layers doped with Ti and V are quite similar. The atomic region surrounding both metals is amorphous in the 'as-deposited' layers and more like carbide after heating at 1100 K.

Tungsten behaves slightly different. The changes in the spectra with temperatures are not so strongly pronounced as for the other three metals for temperatures around 1100 K. Even after heating at 1300 K, the modulations are not as strong as for carbidic tungsten, but already positions in energy are the same. Unfortunately, the reference spectra of WC and of a mixture of WC and W_2C are nearly equal, because the atomic environment in both carbides is nearly equal. A more detailed analysis is necessary to distinguish whether WC or W_2C is created.

4. Discussion and conclusions

The investigated systems, carbon plus about 15 at.% of Ti, V, W, or Zr, were annealed and studied with IBA, XRD, and EXAFS. The metal atoms in the 'as-deposited' doped layers for all four dopants have an amorphous, disordered surrounding which already starts to order at annealing temperatures below 1000 K. Except for tungsten doping, the growing of nanoscopic carbide crystallites is observed. Correlated to that growth, the metal atoms have certain mobility in the carbon matrix. Nevertheless, no diffusion over distances greater than 20 nm is observed.

The phases for Ti, V, and Zr are the predicted ones of carbon-poor TiC, VC, and ZrC, respectively. Tungsten doping leads to the unexpected behaviour, the formation of the tungsten-rich W_2C instead of the stoichiometric WC. But W_2C was also previously observed to be existing between 1000 and 1300 K in photoelectron spectroscopy (XPS) studies on annealed carbon layers on metallic tungsten [27].

The findings about the limited dopant mobility may strongly influence the understanding of the catalytic effect of these metals on the graphitization of carbon. This catalytic effect is explained by the mobility of carbide through the carbon matrix [18]. Graphitization is usually performed at much higher temperatures than used in this study [19]. From graphitization studies of carbon doped with micrometer sized carbide grains [19], tungsten plays a special role: tungsten shows the lowest catalytic effect, which may be correlated with the possibly formation of W_2C.

Acknowledgements

We thank E. de Juan Pardo, I. Quintana, and B.T. Cieciwa for supplying and heating the quintuple layers and generating the knowledge for producing the doped layers. S. Lindig, M. Fußeder, and E. Welter are kindly acknowledged for their technical assistance.

The EXAFS work was supported by the European Community – Research Infrastructure Action under the FP6 'Structuring the European Research Area' Programme (through the Integrated Infrastructure Initiative 'Integrating Activity on Synchrotron and Free Electron Laser Science').

Part of the work has been performed within the framework of the Integrated European Project 'ExtreMat' (Contract NMP-CT-2004-500253) with financial support by the European Community. It only reflects the view of the authors and the European Community is not liable for any use of the information contained therein.

References

[1] International Atomic Energy Agency, Technical Basis for the ITER Final Design, ITER EDA Documentation Series No. 22, IAEA, Vienna, 2001.
[2] International Atomic Energy Agency, ITER Technical Basis, ITER EDA Documentation Series No. 24, IAEA, Vienna, 2002.
[3] V. Barabash, M. Akiba, J.P. Bonal, G. Federici, R. Matera, K. Nakamura, H.D. Pacher, M. Rödig, G. Vieider, C.H. Wu, J. Nucl. Mater. 258–263 (1998) 149.
[4] M. Balden, Phys. Scr. T81 (1999) 64.
[5] A.Y.K. Chen, J.W. Davis, A.A. Haasz, J. Nucl. Mater. 290 (2001) 61.
[6] A.Y.K. Chen, J.W. Davis, A.A. Haasz, J. Nucl. Mater. 312 (2003) 16.
[7] E. Salonen, K. Nordlund, J. Keinonen, C.H. Wu, J. Nucl. Mater. 313–316 (2003) 404.
[8] Q.G. Guo, J.G. Li, N. Noda, Y. Kubota, J.L. Chen, Zh.J. Liu, J.R. Song, J. Nucl. Mater. 313–316 (2003) 144.
[9] K. Nakamura, S. Suzuki, M. Dairaku, K. Yokoyama, Y. Okumura, T. Suzuki, R. Jimbou, V. Bandourko, M. Akiba, J. Nucl. Mater. 263 (1998) 828.
[10] K. Schmid, M. Baldwin, R. Doerner, J. Nucl. Mater. 337 (2005) 862.
[11] J. Roth, A. Kirschner, W. Bohmeyer, S. Brezinsek, A. Cambe, E. Casarotto, R. Doerner, E. Gauthier, G. Federici, S. Higashijima, J. Hogan, A. Kallenbach, H. Kubo, J.M. Layet, T. Nakano, V. Philipps, A. Pospieszczyk, R. Preuss, R. Pugno, R. Ruggieri, B. Schweer, G. Sergienko, M. Stamp, J. Nucl. Mater. 337–339 (2005) 970.
[12] G.F. Counsell, C.H. Wu, Phys. Scr. T91 (2001) 70.
[13] C.H. Skinner, J.P. Coad, G. Federici, Phys. Scr. T111 (2004) 92.
[14] M. Balden, E. de Juan Pardo, H. Maier, P. Starke, U. Fantz, Phys. Scr. T111 (2004) 123.
[15] M. Balden, E. de Juan Pardo, I. Quintana, B. Cieciwa, J. Roth, J. Nucl. Mater. 337–339 (2005) 980.
[16] M. Balden, M. Mayer, J. Nucl. Mater. 298 (2001) 225.
[17] M. Balden, C. Adelhelm, E. de Juan Pardo, J. Roth, J. Nucl. Mater., in press, doi:10.1016/j.jnucmat.2007.01.188.
[18] A. Oya, H. Marsh, J. Mater. Sci. 17 (1982) 309.
[19] N. Ordás, C. García-Rosales, S. Lindig, M. Balden, H. Wang, Phys. Scr. T111 (2004) 190.
[20] M. Balden, B. Cieciwa, I. Quintana, E. de Juan Pardo, F. Koch, M. Sikora, B. Dubiel, Surf. Coat. Technol. 200 (2005) 413.
[21] J.R. Tesmer, M. Nastasi, Handbook of Modern Ion Beam Material Analysis, Material Research Society, Pittsburgh, 1995.
[22] Joint Committee for Powder Diffraction Studies – International Centre for Diffraction Data (JCPDS ICDD), Powder Diffraction File™, Release 2000.
[23] B.D. Cullity, Elements of X-Ray Diffraction, Addison-Wesley, 1967.
[24] D.C. Koningsberger, R. Prins, X-Ray Absorption: Principles, Applications, Techniques of EXAFS, SEXAFS and XANES, Wiley, New York, 1988.
[25] T.B. Massalski (Ed.), Binary Alloy Phase Diagrams, ASM International, Metals Park, Ohio, 1996.
[26] B. Ravel, M. Newville, J. Synchrotron Rad. 12 (2005) 537.
[27] J. Luthin, Ch. Linsmeier, Surf. Sci. 454 (2000) 78.